American Mineralogist, Volume 85, pages 1287–1293, 2000

The crystal structure of $TlAlSiO_4$: The role of inert pairs in exclusion of Tl from silicate minerals

ATSUSHI KYONO,* MITSUYOSHI KIMATA, AND MASAHIRO SHIMIZU

Institute of Geoscience, University of Tsukuba, Tennodai 1-1-1, Tsukubashi, Ibaraki, 305-8571, Japan

ABSTRACT

Thallium aluminosilicate, $TlAlSiO_4$, synthesized hydrothermally is monoclinic with space group $P2_1/n$ [a = 5.4095(3), b = 9.4232(7), c = 8.2629(6) Å, γ = 90.01(2)°, V = 421.20(6) Å^3, Z = 4]. The crystal structure was refined to an R index of 3.8% based on 1852 observed unique reflections. The compound is a unique framework silicate with a topology similar to that of the tridymite structure. The TlO_8 polyhedron resembles a truncated rectangular pyramid, and shares its edges with three adjacent AlO_4 tetrahedra, three SiO_4 tetrahedra, and six TlO_8 polyhedra. Local understaturation at the Tl position suggested by bond-valence analysis implies that lone-pair electrons are present. The geometrical data indicate that the inert pair causes distortion of the Tl-polyhedron. Polyhedral distortion analysis using the software IVTON places the lone-pair parallel to [010], pointing to the largest base of Tl polyhedron. The rule in the valence shell electron pair repulsion model that a nonbonding pair occupies more space on the "surface" of the central atom than a bonding pair supports the orientation of inert-pair electrons in thallium provided by IVTON. The remarkable structure distortion caused by the inert-pair effect explains the rarity of Tl as a major element in silicate minerals because these cannot accommodate extremely distorted polyhedra. In contrast, about forty species of Tl-sulfide minerals exist because these structures are more flexible. Furthermore this effect probably explains why atoms such as Ge^{2+}, Pb^{2+}, Sn^{2+}, Sb^{3+}, and Bi^{3+}, crystallize not as silicate phases but mainly as sulfide ones in nature.

INTRODUCTION

The low content of thallium in the Earth's crust and its geochemical similarity to potassium and rubidium promote dispersion of this element in endogenic rocks and ore formation (Mason 1966). Recent surveys on the production of subduction-related magmas (Noll et al. 1996) and the origin of Cu-Au porphyry deposits (Kamenetsky et al. 1999) reported efficient mobilization of thallium into arc magma source regions. However, thallium is sequestered in sulfide minerals, e.g., lorandite $TlAsS_2$, vrbaite $Hg_3Tl_4Sb_2As_8S_{20}$, and hutchinsonite $(Pb,Tl)_2As_5S_9$ (Clark 1993). The only silicate minerals containing major element concentrations of Tl are Tl-bearing ammonioleucites (Nishida et al. 1997) for which the crystal structure was determined by Rietveld refinements of synthetic $TlAlSiO_4$ (Krogh et al. 1991), and a thallium-leucite pseudomorph after analcime, $TlAlSi_2O_6$ (Kyono et al. 1999), which was identified by X-ray powder diffraction.

Even though Tl^+ is similar to K^+ and Rb^+ in chemical properties and ionic size (Shannon 1976), the distinguishing characteristics of Tl depends on an inert-pair effect. The heavier members of Group 13 and 14 develop a valency two less than the normal valency, and distortion along one axis of the M-centered polyhedron often occurs due to the influence exerted by the lone pair (Cotton and Wilkinson 1988; Downs 1993). Large cations with stereochemically active lone-pair electrons (such as Tl^+, Pb^{2+}, Sn^{2+}, and Bi^{3+}) have received particular attention owing to their interesting structural features and physical properties (see Gillespie 1972; Moore and Araki 1976; Hawthorne and Groat 1986; Merlino et al. 1993; Cooper and Hawthorne 1995; Cooper et al. 1999 and references therein). The polyhedral distortions that result due to a ns^2 lone pair (n = 5, 6) of electrons in the valence shell of the central cation were discussed in detail by Gillespie (1972). Lone-pair effect in the coordination polyhedron in minerals has been studied for about Pb^{2+}, Sb^{3+}, and As^{3+} (e.g., Moore 1988; Moore and Araki 1976; Araki and Moore 1981). This paper determines the crystal structure of $TlAlSiO_4$ using single-crystal X-ray diffraction and examines if the inert-pair effect causes exclusion of thallium from silicate minerals.

EXPERIMENTAL METHODS

Standard cold-seal hydrothermal techniques were used to synthesize $TlAlSiO_4$ crystals. About 10 mg of low albite ($Ab_{98.8}An_{1.0}$) from Minas Gerais, Brazil was mixed with over 200 mg thallium nitrate and poured into a silver tube 20 mm long and 5 mm diameter). Distilled water was added to give a 70% filling ratio before sealing the tube. The silver tube was heated in an autoclave up to 500 °C for 14 days. Temperature was recorded with Pt/Pt13Rh thermocouples closely adjoining the sample position. Vapor pressure during the synthesis was estimated as 60 MPa. The experiments were stopped by allowing the autoclaves to gradually re-equilibrate to room temperature.

*E-mail: kyono@arsia.geo.tsukuba.ac.jp

The morphology of the synthesized samples was examined by optical and scanning electron microscopy (SEM). Each product was polished to a thin section and examined under a high-magnification polarizing microscope. SEM photographs of the synthesized Tl-aluminosilicate show an idiomorphic mineral although these crystals were too small to index the habit.

Chemical compositions were determined using wavelength-dispersion spectroscopy (WDS) on a JEOL superprobe (JXA-8621) operating at 20 kV and 10 nA, with a beam diameter of 10 μm. Data reduction was carried out using the ZAF procedure. The concentration of Ca was measured using $CaSiO_3$ as the standard (Ca$K\alpha_1$). The elements Mg, Fe, Ti, Mn, Ni, and Cr were sought, but not detected. Initial analysis of the major elements (Tl, K, Na, Al, Si) was carried out using the synthetic lorandite (Tl$M\alpha_1$) (Berlepsch 1996), microcline (K$K\alpha_1$), albite (Na$K\alpha_1$), corundum (Al$K\alpha_1$) and quartz (Si$K\alpha_1$) as standards. The accuracy of standard was then tested by cross-analysis with well-characterized minerals. The representative compositions are shown in Table 1. The empirical formula calculated on the basis of four oxygen atoms is $(Tl_{0.956}\square_{0.044})Al_{0.956}Si_{1.044}O_4$, which is close to endmember $TlAlSiO_4$.

Crystallographic results and discussion

The X-ray powder diffraction patterns were obtained using a RIGAKU diffractometer FR-552 (Cu$K\alpha_1$ radiation, flat graphite monochromator, 2θ step = 0.02°, scintillation counter, with silicon as an internal standard). The X-ray powder diffraction pattern (Table 2) was indexed on a monoclinic lattice, using the cell parameters from the single crystal data (Table 3). The values of the cell parameters and the XRD pattern are similar to those of the $Tl_{1.1}AlSiO_4$ (in an ABW-type structure) reported by Krogh et al. (1991). However, the crystal structure of $Tl_{1.1}AlSiO_4$ which Krogh et al. (1991) determined by Rietveld refinement posed several crystal-chemical problems: (1) The Tl cation on the extra framework site occupies three partially populated positions, (2) their structural formula has an excess 0.1 charge, (3) the positions where the T1 ions are located have curiously irregular surroundings, and (4) the other atoms have abnormal isotropic temperature parameters. These problems prompted redetermination of the crystal structure of $TlAlSiO_4$.

Structural solution and refinement. X-ray intensity data for $TlAlSiO_4$ were collected on the Enraf-Nonius CAD-4 diffractometer utilizing graphite-monochromated Mo$K\alpha$ radia-

TABLE 1. Chemical analyses

	Theoretical	Measured
SiO_2	18.58	19.83
Al_2O_3	15.76	15.50
Tl_2O	65.66	64.35
Total (wt%)	100.00	99.68
	Cations*	
Si	1.000	1.042
Al	1.000	0.959
Tl	1.000	0.956
Total	3.000	2.957

* Based on 4 O atoms.

TABLE 2. X-ray powder diffraction data

h	k	l	I/I_0	d_{obs} (Å)	d_{calc} (Å)*
0	1	1	8	6.21	6.21
1	1	0	26	4.69	4.69
$\bar{1}$	1	0			
0	0	2	12	4.13	4.13
1	2	1	56	3.264	3.264
1	$\bar{2}$	1			
$\bar{1}$	1	2	100	3.103	3.101
0	3	1	40	2.936	2.936
$\bar{1}$	3	0	18	2.716	2.717
1	3	0			
$\bar{2}$	0	0	22	2.703	2.704
0	$\bar{1}$	3	8	2.644	2.644
2	$\bar{1}$	1	2	2.480	2.480
2	1	$\bar{1}$			
$\bar{2}$	2	0	14	2.346	2.346
2	2	0			2.345
$\bar{1}$	3	2	6	2.269	2.270
1	3	$\bar{2}$			
2	0	2	12	2.262	2.263
$\bar{1}$	2	3	10	2.177	2.177
1	2	3			
$\bar{1}$	4	1	24	2.090	2.090
1	4	$\bar{1}$			
0	3	$\bar{3}$	24	2.071	2.071
0	0	$\bar{4}$	14	2.066	2.066
$\bar{2}$	2	2	10	2.039	2.040
2	2	2			
2	$\bar{3}$	1	24	1.989	1.989
2	3	1			
0	$\bar{2}$	4	22	1.891	1.892
$\bar{2}$	1	3			1.891
0	5	$\bar{1}$	18	1.837	1.836
$\bar{1}$	5	0	4	1.780	1.780
1	5	0			
$\bar{3}$	1	0	4	1.771	1.771
3	1	0			
1	4	3	26	1.700	1.700
1	4	3			
3	$\bar{2}$	1	8	1.650	1.650
3	2	1			
$\bar{2}$	3	3	14	1.644	1.644
1	3	$\bar{4}$			
2	0	$\bar{4}$	10	1.642	1.642
3	$\bar{1}$	2	12	1.627	1.628
0	6	0	2	1.570	1.571
3	$\bar{3}$	0	4	1.563	1.564
3	3	0			
0	5	$\bar{3}$	4	1.555	1.556
$\bar{2}$	2	4	6	1.550	1.550
2	2	$\bar{4}$			
$\bar{2}$	5	1	10	1.520	1.520
2	5	$\bar{1}$			
1	$\bar{2}$	5	10	1.499	1.499
$\bar{1}$	6	1	6	1.484	1.484
1	6	1			
0	$\bar{6}$	2	4	1.468	1.468

—Continued next page

TABLE 2—*Continued*

h	k	l	I/I_0	d_{obs} (Å)	d_{calc} (Å)*
3	$\bar{3}$	2			
			6	1.463	1.463
0	3	5			
3	$\bar{2}$	3			
			2	1.436	1.437
3	2	3			
$\bar{3}$	4	1			
			4	1.411	1.411
3	4	$\bar{1}$			
0	0	$\bar{6}$	2	1.378	1.377
$\bar{4}$	0	0	4	1.352	1.352
$\bar{2}$	5	3			
			6	1.348	1.348
1	5	$\bar{4}$			
$\bar{3}$	1	4	4	1.345	1.345
0	$\bar{7}$	1	2	1.329	1.329
0	2	$\bar{6}$			1.322
			8	1.323	
4	$\bar{1}$	1			1.321
1	$\bar{4}$	5	4	1.313	1.313
1	$\bar{7}$	0			
			4	1.306	1.306
1	7	0			
3	$\bar{5}$	0			
			2	1.303	1.303
3	5	0			
1	$\bar{7}$	1			
			6	1.290	1.290
1	7	$\bar{1}$			
$\bar{2}$	3	5	6	1.287	1.287
$\bar{3}$	4	3			1.271
			6	1.270	
3	4	$\bar{3}$			1.270
0	6	$\bar{4}$	2	1.251	1.250
$\bar{1}$	7	2	4	1.246	1.246
$\bar{3}$	5	2			
			6	1.243	1.243
0	5	5			
$\bar{4}$	2	2			
			4	1.240	1.240
4	2	2			
$\bar{4}$	3	1			
			6	1.228	1.228
1	3	$\bar{6}$			
0	$\bar{7}$	3	2	1.210	1.210
$\bar{4}$	1	3	2	1.204	1.204

* d_{cal} based on refined cell parameters: a = 5.4090(3), b = 9.4236(5) Å, c = 8.2644(6) Å, γ = 90.006(6)°, V = 421.26(3).

tion for the hemisphere of reciprocal space encompassing $k > 0$. Initial investigation on the diffractometer indicated the presence of only reflections allowed by a P-lattice. Intensity data were collected to $\theta = 35°$ with $\omega/2\theta$ scans with a scan angle of $\omega = 1.6°/s$ plus a correction for dispersion. An electron microprobe analysis, subsequent to measurement of the intensity data, showed that the crystal was homogeneous. Crystal-structure refinements were done with occupancies fixed at the chemical compositions given by electron microprobe results. The experimental details are given in Table 3. An empirical absorption correction was applied using the ψ-scan technique. Data reduction, including background and Lorenz-polarization corrections, was performed with the SDP program (Enraf-Nonius 1983). The program SHELXL-97 (Sheldrick 1997) was used for refinement of the structure in space group $P2_1/n$. Neutral atom scattering factors were used in all refinements. Starting coordinates were taken from the structure of $CsLiSO_4$ at –100 °C (Asahi and Hasebe 1988), and the structure was refined with a single site model for the Tl position, which successfully converged to R = 3.8%. Final positions, displacement parameters, selected interatomic distances are given in Tables 4, 5, and 6.

TABLE 3. Crystal data

Dimensions		0.10 × 0.12 × 0.07 mm³
Space group		$P2_1/n$
Unit cell	a	5.4095(3) Å
	b	9.4232(7) Å
	c	8.2629(6) Å
	γ	90.01(2)°
	V	736.9(2) Å³
	Z	4
Calculated density		4.959 g/cm³
μ (Mo$K\alpha$)		1.73 mm⁻¹
θ limits		≦0.05–30°
Data collected		2052
Unique data		1852
Data > $4\sigma_1$		1250
Scan type		$\theta/2\theta$
Scan time		≦70 s
R_{merge}		0.054
R		0.038

Description of the structure. The crystal structure of $TlAlSiO_4$ refined using the $CsLiSO_4$ model is isostructural with that of $RbAlSiO_4$ (Klaska and Jarchow 1975). $TlAlSiO_4$ exhibits the isotype with the *Icmm*-type framework of $RbAlSiO_4$, belonging to the series $M[AlSiO_4]$ classified by Liebau (1985). The present compound has a silicate framework similar to that of tridymite, i.e., a framework constructed of zweier chains with all tetrahedra pointing up alternating with zweier chains with all tetrahedra pointing down. The staggered Al-O-Si angles of 174.3° for $TlAlSiO_4$ are similar to the Li-O-S angles for $CsLiSO_4$, but differ markedly from those of 151.1° in $RbAlSiO_4$ (Fig. 1). The mean Al-O distance is 1.734 Å, and the mean Si-O distance is 1.611 Å. In spite of the extreme distortion of M-polyhedron, these bond distances indicate a well-ordered framework composed of Al and Si tetrahedra (Jones 1968). Ordering into alternation of SiO_4 and AlO_4 tetrahedra follows Loewenstein's aluminum avoidance rule (Loewenstein 1954).

The present crystal structure, exclusive of the Tl site, is approximately consistent with the structural data for $TlAlSiO_4$ determined by Krogh et al. (1991). The fundamental building blocks (Hawthorne 1992) in this crystal are the $SiAlO_7$ pyroanions of an eclipsed type along [100] and [001] and those of a staggered type along [010], polymerization of which leads to formation of the framework silicate. One can view the slabs as consisting of alternating up- and down-tetrahedral chains, parallel to [100] (Fig. 1). Two-dimensional polymerization of those two kinds of pyroanions can be regarded as the six-mem-

TABLE 4. Atomic coordinates and isotropic temperature factors

Atom	x	y	z	U_{eq}
Tl	0.7502(1)	0.1891(1)	0.4973(1)	0.0339(3)
Si	0.2503(6)	0.0765(4)	0.2052(4)	0.0233(6)
Al	0.2490(6)	0.4168(3)	0.3082(4)	0.0118(6)
O1	0.2500(22)	0.0657(17)	0.0140(10)	0.0349(27)
O2	0.2447(24)	0.2379(10)	0.2639(19)	0.0546(45)
O3	0.0066(15)	0.9982(9)	0.2788(15)	0.0294(21)
O4	0.4932(13)	–0.0012(9)	0.2824(13)	0.0256(19)

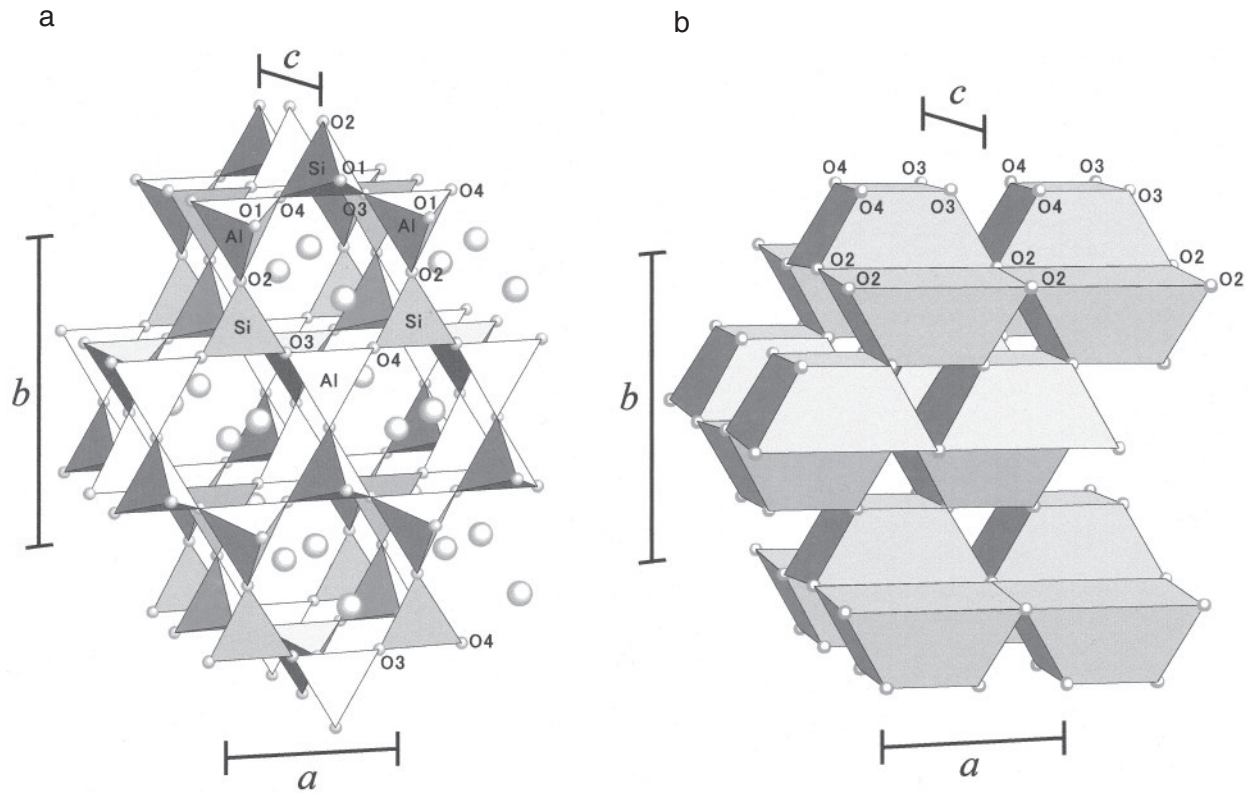

FIGURE 1. (**a**) Projection of the crystal structure of $TlAlSiO_4$ parallel to [001] direction. The layers of the six-membered rings approximately perpendicular to [001] belong to the so-called Icmm-type (Liebau 1985). The staggered T_2O_7 pyroanions (T = Al,Si) are paralleled to [010] direction, and the eclipsed ones are paralleled to [001] direction. Tl atoms are shown by spheres. (**b**) The partial structure projected along [001] shown TlO_8 polyhedron shares six edges with Tl polyhedra and six edges with Si and Al tetrahedra.

bered ring layers, and their stacking forms honey-comb-like nets in the (001) planes. Linkage of the fundamental layers vertical to [001] leads to the framework composed of all six-membered rings centered aligned on [001].

The important characteristic of the $TlAlSiO_4$ structure is the Tl coordination at the M site surrounded by eight O atoms, forming a trapezohedral polyhedron like a truncated rectangular pyramid (Fig. 2). The Tl-O bond lengths are divided into two groups: the short distance group ranges from 2.87 to 2.90 Å (mean 2.88 Å) and the long distance group ranges from 3.34 to 3.57 Å (mean 3.46 Å). This type of asymmetrical coordination is typical for lone-pair-stereoactive Tl^+ (West 1999). The compression along [010] of Tl-polyhedron is a consequence of the stereoactive lone pair of electrons originated from Tl^+ ions. The stereochemically active lone pair of electrons also manifests itself in the bond lengths, with a considerable increase in the Tl-O2 bond length relative to that of Tl-O3 and Tl-O4. The framework of the crystal structure accommodates chains of edge-shared TlO_8 polyhedra (Fig. 1). The extremely large isotropic temperature factor for O2 suggests hexacoordinated O2; that is the bridging oxygen O2 is in a staggered $SiAlO_7$ configuration.

The bond valence sums around the total cation sites (Table 7) are in good agreement with the aggregate charge around each anion (S = 8.08), which result in the approximate electrostatic cancellation of negative and positive deviations (Brese and O'Keeffe 1991). The sum of the bond valence to the coordinating anions around the Tl site represents a marked deficiency in

TABLE 5. Anisotropic displacement parameters

Atom	U_{11}	U_{22}	U_{33}	U_{12}	U_{13}	U_{23}
Tl	0.0428(5)	0.0260(4)	0.0328(4)	0.0008(3)	–0.0002(2)	0.0010(2)
Si	0.0236(14)	0.0231(14)	0.0231(14)	0.0002(11)	–0.0021(10)	0.0006(11)
Al	0.0106(12)	0.0106(12)	0.0140(12)	0.0021(9)	0.0001(9)	–0.0018(9)
O1	0.0263(45)	0.0611(88)	0.0172(38)	0.0017(48)	–0.0015(28)	–0.0018(36)
O2	0.0713(104)	0.0172(46)	0.0754(115)	0.0167(56)	0.0128(88)	0.0014(61)
O3	0.0274(44)	0.0334(52)	0.0275(52)	–0.0034(37)	0.0020(28)	–0.0044(30)
O4	0.0198(37)	0.0368(52)	0.0202(42)	0.0131(34)	0.0022(23)	0.0012(27)

TABLE 6. Interatomic distances (Å) and interatomic angles (°)

Si-O1	1.583(9)	O1-Si-O2	111.3(8)	Tl-O4'	2.87(1)
Si-O2	1.597(11)	O1-Si-O3	110.1(7)	Tl-O4''	2.87(1)
Si-O3	1.628(9)	O1-Si-O4	111.2(6)	Tl-O3'	2.87(1)
Si-O4	1.634(8)	O2-Si-O3	107.6(6)	Tl-O3''	2.90(1)
Mean	1.611	O2-Si-O4	108.9(6)	Tl-O2'	3.34(1)
		O3-Si-O4	107.6(5)	Tl-O2''	3.36(1)
		Mean	109.5	Tl-O2'''	3.55(1)
				Tl-O2''''	3.57(1)
				Tl-O3'''	3.93(1)
				Tl-O4'''	3.96(1)
				Tl-O4''''	4.00(1)
				Tl-O3''''	4.01(1)
Al-O1	1.709(9)	O1-Al-O2	107.8(6)	Mean	3.44
Al-O2	1.725(10)	O1-Al-O2	111.4(6)		
Al-O3	1.745(10)	O1-Al-O3	112.6(5)	Si-O1-Al	170.8(9)
Al-O4	1.753(9)	O1-Al-O4	110.7(6)	Si-O2-Al	174.3(9)
Mean	1.733	O2-Al-O3	109.2(5)	Si-O3-Al	133.7(8)
		O3-Al-O4	105.1(5)	Si-O4-Al	131.7(7)
		Mean	109.5	Mean	152.6

TABLE 7. Bond valence sums

	O1	O2	O3	O4	S*V*
Si	1.12	1.08	0.99	0.97	4.16
Al	0.85	0.82	0.77	0.76	3.20
Tl	0.02↓	0.04	0.15	0.15	0.72
	0.02↓	0.04	0.14	0.15	
	0.02↓	0.02↓			
		0.02↓			
		0.03→			
		0.02→			
Σ*V*	2.03	2.02	2.05	2.03	

Note: Bond valences (express in valence units) were calculated from the curve of Brese and O'Keeffe (1991).

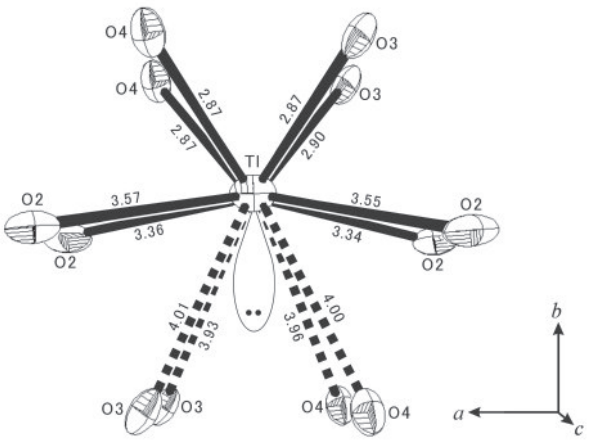

FIGURE 2. Tl-O coordination environment and bond distances (Å).

electrostatic balance. Both structural distortion of the polyhedron and its deficiency in the bond balance sum are linked to non-bonding electron effects, which are grouped into two types: the *d* electrons in transition metal compounds and the s^2 pair of electrons in compounds of the heavy *p*-block elements in low oxidation states (West 1999). The latter is referred to as so-called the inert-pair effect. Thus the extremely irregular polyhedron of Tl^+ cation can be explained by the inert-pair effect (Cotton and Wilkinson 1988; Downs 1993). Orientation of the lone-pair electrons of Tl^+ may account for the larger temperature factor of O2 constituting four apexes of the Tl-polyhedron. Similarly, large temperature factors of O atoms are seen in the Pb-O polyhedra (e.g., Moore et al. 1982, 1989). An abnormality in thermal parameters of ligands is consistent with one of the crystal-chemical characteristics caused by the inert-pair effect.

A comparison of distorted $BiMnO_3$ with $LaMnO_3$ ($GdFeO_3$-type structure), showed that the inert-pair effect of Bi^{3+} tolerates the lower symmetry of the latter structure (Atou et al. 1999). The lowering of the structure symmetry from orthorhombic in the case of $RbAlSiO_4$ (Klaska and Jarchow 1975) to monoclinic for $TlAlSiO_4$ is, apparently, caused by the inert-pair effect of the Tl^+ cation. The observation that compounds having cations with lone-pair electrons are of lower symmetry than the isotypic ones without such cations may hold in general.

Orientation of inert-pair electrons

It is not easy to extract meaningful information about the position of the inert-pair electrons. The sphericity and eccentricity parameters calculated with the computer program IVTON (Balic-Zunic and Vickovic 1996) are listed in Table 8 for the purpose of inferring the position of inert-pair electrons. Our approach arose also from the need to accommodate nonspherical ions into the Brown model used to determine the bond valence sum of Tl cations. The IVTON's parameters are a measure of the degree of deformation of the coordination polyhedra and can provide hints as to site preferences. The sphericity value (*s*) of the KO_9 polyhedra in $KAlSiO_4$ is the highest ($s = 0.997$), while RbO_8 polyhedra in $RbAlSiO_4$ show the lowest sphericity ($s = 0.940$) indicative of the most irregular polyhedra in these compounds. The sphericities of any coordination polyhedra are related to the centroid-centered atom distance, namely cation eccentricity, which is the displacement D of the central atom from the "best" center of the ligand arrangement. The direction of this displacement is assumed to be opposite to the orientation of the lone pair on this atom (Balic-Zunic and Makovicky 1996). Consequently, large cations in the extraframework sites yield low sphericity and high eccentricity values on account of the low symmetry of their framework structures. It is noteworthy, however, that the crystal structure of $TlAlSiO_4$ has an extremely large eccentricity value ($d = 0.779$ Å) in spite of the large cation size of Tl. This marked deviation from the centroid implies that the distorted coordination could be caused by the stereochemical activity of the Tl^+ lone-pair electrons.

The eightfold coordination polyhedra of Tl can be regarded as a truncated rectangular pyramid compressed along [010] (Fig. 1). The compression along [010] is a consequence of the stereoactive lone pair of electrons associated with Tl^+ ions. The stereochemically active lone pair of electrons also manifests itself in the bond lengths, with a considerable increase in the Tl-O2 bond length relative to those of Tl-O3 and Tl-O4. In the valence shell electron pair repulsion (VSEPR) model (McKenna and McKenna 1984), a nonbonding pair occupies more space on the "surface" of the central atom than a bonding pair (Cot-

TABLE 8. Selected polyhedral parameters for the atoms (Tl, K, Rb)

	CN	*V* (Å³)	*r* (Å)	*d* (Å)	*s*	Reference
$TlAlSiO_4$	8	37.43	3.414	0.779	0.986	This study
$RbAlSiO_4$	8	43.47	3.171	0.067	0.940	Klaska and Jarchow (1975)
$KAlSiO_4$	9	46.66	2.968	0.008	0.997	Dollase and Freeborn (1977)

Notes: CN = coordination number; *V* = Volumes of coordination polyhedron; *r* = mean distance from centroid to ligands; *d* = centroid-central atom distance; *s* = sphericity of coordination polyhedron.

ton and Wilkinson 1988). The IVTON calculations allow us to expose the difference in eccentricity between the polyhedra of an eightfold-coordination and a 12-fold one (Fig. 2), where their apexes are oxygen atoms. The latter eccentricity underscores the validity of the VSEPR model for the lone-pair electrons. Addition of these two IVTON and VSEPR constraints to thermal parameters of the bridging O2 in the staggered $SiAlO_7$ pyroanions orientated and stacked along [010] bears witness to the space which the non-bonding pair of electrons takes up. This [010] orientation of the Tl-lone pair electrons gives rise to a novel framework for $TlAlSiO_4$. To reduce steric repulsion between the lone pairs of adjacent Tl ions in the edge-shared eightfold-coordinated blocks, the ions adopt a zigzag arrangement along [001], namely the [001] tetrahedral chain that a Tl polyhedron pointing up continues to alternate with that pointing down. The similar zigzag arrangement of unusually distorted polyhedra due to the tendency of ns^2 lone pair is exemplified in the $K_2Gd_2Sb_2Se_9$ compound by the zigzag arrangement of the Sb atoms caused by the steric requirements of the 5s^2 lone pair of adjacent Sb ions in the edge-shared octahedral blocks (Choi et al. 1999).

Abnormal coordination of thallium ions: Inert-pair effect

One mystery still left to be clarified about Tl^+ is the necessity for distortion of the polyhedra due to the inert-pair effect: in cases where Tl has the same coordination numbers, there is greater polyhedral distortion for silicates than for sulfides (Kyono et al. 1999). $TlAlSiO_4$ exhibits a framework structure accommodating an extremely distorted TlO_8 polyhedron (Fig. 2) with the Tl-O bond lengths ranging from 2.87 to 3.57 Å (spread of 0.70 Å), whereas the framework of $RbAlSiO_4$ contains RbO_{11} polyhedra with the Rb-O bond lengths ranging from 2.910 to 3.537 Å (Klaska and Jarchow 1975). In thallium borate TlB_3O_5, there are unique polyhedra where six O atoms are around Tl^+ at distances between 2.662 and 3.198 Å (spread of 0.536 Å) (Touboul et al. 1997). This Tl-polyhedron is significantly different from that of Cs^+ in CsB_3O_5, with Cs-O distances between 3.030 and 3.342 Å (spread of 0.312 Å) (Krong-Moe 1974), even though Cs^+ has a larger ionic radius than Tl^+ (Shannon 1976). The greater distortion of the Tl-polyhedron in $TlAlSiO_4$ is typical of Tl-O polyhedra in crystal structures (Wells 1987). In thallium sulfides or thallium sulfates, however, the inert-pair effect becomes very little. For instance, the Tl-S distances vary between 3.211 and 3.373 Å (spread of 0.162 Å) in edenharterite, $PbTlAs_3S_6$ (Berlepsch 1996), and the Tl-O(OH) distances between 2.937 and 3.095 Å (spread of 0.158 Å) in dorallcharite, $(Tl,K)Fe^{3+}_3(SO_4)_2(OH)_6$ (Zunic et al. 1994). Despite the presence of a lone electron pair, there are more uniform distributions of the Tl-S or Tl-O(OH) distances in the Tl polyhedra. Moreover, thallium is more electronegative than the alkali metals and tends to form compounds with polarizable anions, as does silver (Deubener et al. 1991). The difference in the electronegativities of Tl (1.8) and S (2.5) or O (3.5) indicates the low ionicity of Tl-S bond relative to Tl-O. Hence, in silicates or borates the polyhedral distortion due to the inert-pair effect is pronounced at Tl sites, while in sulfides or sulfates it is minimized.

The inert-pair effect of Tl^+ cation in the $TlAlSiO_4$ structure may be increased because the bridging anion of the Si-O-Si dimer in the feldspar framework exhibits only one localized nonbonded lone electron pair (Gibbs et al. 1998), and the chemical bonds between Tl^+ and its surrounding O^{2-} are underlied by the hard-soft acid-base (HSAB) principle (Douglas et al. 1994). A hard acid prefers to combine with a hard base, and a soft acid prefers to combine with a soft base. Inasmuch as soft acid-base interactions involve significant polarization (covalence), soft acids (e.g., Ag^+, Hg^+, Tl^+) and hard bases (e.g., F^-, OH^-, O^{2-}) bind electrons tightly, and thus the electron clouds cannot be easily distorted or polarized. This behavior causes extreme distortion of TlO_8 polyhedra, as in $TlAlSiO_4$. Therefore, both the reciprocal interactions between lone-pair electrons due to an inert-pair effect and localized nonbonded lone electron pairs present in the bridging O atoms leads to our interpretation that it may be highly characteristic of Tl^+ cations to have extremely distorted oxypolyhedra in the polymerized aluminosilicates.

Geological implications

Prior to this study, little was known about factors that give rise to the rare occurrence of thallium-silicate minerals in nature. This study shows that $TlAlSiO_4$ has extremely distorted polyhedra caused by the inert-pair effect of Tl atoms, and it is likely that the effect is manifested to a greater degree in silicates as opposed to sulfides. The inert-pair effect is generally known for Ge^{2+}, Pb^{2+}, Sb^{3+}, Sn^{2+}, and Bi^{3+} (Cotton and Wilkinson 1988), and many minerals having these cations as major constituents crystallize as sulfides in nature, e.g., briartite Cu_2FeGeS_4 (Wintenberger 1979), galena PbS (Noda et al. 1987), stibnite Sb_2S_3 (Bayliss and Nowacki 1972), stannite Cu_2FeSnS_4 (Hall et al. 1978), and pavonite $AgBi_3S_5$ (Makovicky et al. 1977).

ACKNOWLEDGMENTS

We appreciate S. Shimoda, the University of Tsukuba, for his encouragement. Thanks are due to S. Takizawa for guidance in scanning electron microscopy, to N. Nishida for guidance in electron-microprobe analysis, and to S. Saito for setting up the electric furnace. T. Hatta provided help with the X-ray powder diffraction work. The authors also thank P. Berlepsch, Universitat Basel, Switzerland, who generously provided lorandite synthesized for the standard of thallium by EPMA. We are indebted to T. Balich-Zunich, University of Copenhagen, Denmark, for providing the IVTON-program that was necessary for the completion of this work. Helpful reviews by J.M. Hughes and G.E. Harlow resulted in improvements to the manuscript.

REFERENCES CITED

Araki, T. and Moore, P.B. (1981) Dixenite, $Cu^{1+}Mn^{2+}_{14}Fe^{3+}(OH)_6(As^{3+}O_3)_5(Si^{4+}O_4)_2(As^{5+}O_4)$: metallic $[As^{3+}_4Cu^{1+}]$ clusters in an oxide matrix. American Mineralogist, 66, 1263–1273.

Asahi, T. and Hasebe, K. (1988) X-ray study of $LiCsSO_4$ in connection with its ferroelastic phase transition. Journal of the Physical Society of Japan, 57, 4184–4190.

Atou, T., Chiba, H., Ohoyama, K., Yamaguchi, Y., and Syono, Y. (1999) Structure determination of ferromagnetic perovskite $BiMnO_3$. Journal of Solid State Chemistry, 145, 639–642.

Balic-Zunic, T. and Vickovic, I. (1996) IVTON—program for the calculation of geometrical aspects of crystal structures and some crystal chemical applications. Journal of Applied Crystallography, 29, 305–306.

Balic-Zunic, T. and Makovicky, E. (1996) Deformation of the centroid or 'the best center' of a coordination polyhedron. Acta Crystallographica, B52, 78–81.

Bayliss, P. and Nowacki, W. (1972) Refinement of the crystal structure of stibnite, Sb_2S_3. Zeitschrift für Kristallographie, 135, 308–315.

Berlepsch, P. (1996) Crystal structure and crystal chemistry of the homeotypes edenharterite ($TlPbAs_3S_6$) and jentschite ($TlPbAs_2SbS_6$) from Lengenbach, Binntal (Switzerland). Schweizerische Mineralogische und Petrographische Mitteilungen, 76, 147–157.

Brese, N.E. and O'Keefee, M. (1991) Bond-valence parameters for solids. Acta Crystallographica, B47, 192–197.

Choi, K.S., Hanko, J.A., and Kanatzidis, M.G. (1999) Eightfold superstructure in $K_2Gd_2Sb_2Se_9$ and $K_2La_2Sb_2S_9$ caused by three-dimensional ordering of the $5s^2$ lone pair of Sb^{3+} ions. Journal of Solid State Chemistry, 147, 309–319.

Clark, A.M. (1993) Hey's mineral index: mineral species, varieties and synonyms, 3rd ed., 848 p. Chapman and Hall, London.

Cooper, M.A. and Hawthorne, F.C. (1995) Diaboleite, $Pb_2Cu(OH)_4Cl_2$, a defect perovskite structure with stereoactive lone-pair behavior of Pb^{2+}. Canadian Mineralogist, 33, 1125–1129.

Cooper, M.A., Hawthorne, F.C., Merlino, S., Pasero, M., and Perchiazzi, N. (1999) Stereoactive lone-pair behavior of Pb in the crystal structure of bideauxite: $Pb^{2+}_2Ag^+Cl_3F(OH)$. Canadian Mineralogist, 37, 915–921.

Cotton, F.A. and Wilkinson, G. (1988) Advanced inorganic chemistry, 5th ed., p. 22–27 and p. 208–209. Wiley, New York.

Deubener, J., Sternitzke, M., and Müller, G. (1991) Feldspars $MAlSi_3O_8$ (M = H, Li, Ag) synthesized by low-temperature ion exchange. American Mineralogist, 76, 1620–1627.

Dollase, W.A. and Freeborn, W.P. (1977) The structure of $KAlSiO_4$ with $P6_3mc$ symmetry. American Mineralogist, 62, 336–340.

Douglas, B.E., McDaniel, D.H., and Alexander, J.J. (1994) Concepts and Models of Inorganic Chemistry, 3rd ed., 928 p. Wiley, New York.

Downs, A.J. (1993) Chemistry of aluminium, gallium, indium and thallium, 526 p. Blackie Academic & Professional, London.

Enraf-Nonius (1983) Structure determination package (SDP). Enraf-Nonius, Delft, The Netherlands.

Gibbs, G.V., Boisen, M.B., Hill, F.C., Tamada, O., and Downs, R.T. (1998) SiO and GeO bonded interactions as inferred from the bond critical point properties of electron density distributions. Physics and Chemistry of Minerals, 25, 574–584.

Gillespie, R.J. (1972) Molecular geometry, p. 6–15. Van Nostrand-Reinhold, London.

Hall, S.R., Szymańsky, J.T. and Stewart, J.M. (1978) Kesterite, $Cu_2(Zn,Fe)SnS_4$, and stannite, $Cu_2(Fe,Zn)SnS_4$, structurally similar but distinct minerals. Canadian Mineralogist, 16, 131–137.

Hawthorne, F.C. (1992) Bond topology, bond valence, and structure stability. In The Stability of Minerals, Edited by G.D. Price and N. L. Ross, 368 p. Chapman and Hall, London.

Hawthorne, F.C. and Groat, L.A. (1986) The crystal structure and chemical composition of cumengéite. Mineralogical Magazine, 50, 157–162.

Jones, J.B. (1968) Al-O and Si-O tetrahedral distances in aluminosilicate framework structures. Acta Crystallographica, B24, 355–358.

Kamenetsky, V.S., Wolfe, R.C., Eggins, S.M., Mernagh, T.P., and Bastrakov, E. (1999) Volatile exsolution at the Dinkidi Cu-Au porphyry deposit, Philippines: A melt-inclusion record of the initial ore-forming process. Geology, 27, 691–694.

Klaska, R. and Jarchow, O. (1975) Die kristallstruktur und die verzwillingung von $RbAlSiO_4$. Zeitschrift für Kristallographie, 142, 225–238.

Krogh, A.I.G., Krogh, A.E., Norby, P., Colella, C., and de'Gennaro, M. (1991) Synthesis and structure of an ABW type thallium aluminosilicate. Zeolites, 11, 149–154.

Krong-Moe, J. (1974) Refinement of the crystal structure of cesium triborate, $Cs_2O{\cdot}3B_2O_3$. Acta Crystallographica, B30, 1178–1180.

Kyono, A., Kimata, M., Shimizu, M., Saito, S., Nishida, N., and Hatta, T. (1999) Synthesis of thallium-leucite ($TlAlSi_2O_6$) pseudomorph after analcime. Mineralogical Magazine, 63, 75–83.

Liebau, F. (1985) Structural Chemistry of Silicates, 347 p. Springer-Verlag, Berlin.

Loewenstein, W. (1954) The distribution of aluminium in the tetrahedra of silicates and aluminates. American Mineralogist, 39, 92–96.

Makovicky, E., Mumme, W.G., and Watts, J.A. (1977) The crystal structure of synthetic pavonite, $AgBi_3S_5$, and the definition of the pavonite homologous series. Canadian Mineralogist, 15, 339–348.

Mason, B. (1966) Principles of geochemistry, 3rd ed., 329 p. Wiley, New York.

McKenna, A.G. and McKenna, J. F. (1984) Teaching VSEPR theory: the dilemma of five-coordination. Journal of Chemical Education, 61, 771–773.

Merlino, S., Pasero, M., and Perchiazzi, N. (1993) Crystal structure of paralaurionite and its OD relationships with laurionite. Mineralogical Magazine, 57, 323–328.

Moore, P.B (1988) The joesmithite enigma: Note on the $6s^2$ Pb^{2+} lone pair. American Mineralogist, 73, 843–844.

Moore, P.B. and Araki T. (1976) Derbylite, $Fe^{3+}_4Ti^{4+}_3Sb^{3+}O_{13}(OH)$, a novel close-packed oxide structure. Neues Jahrbuch für Mineralogie. Abhandlungen, 126, 292–303.

Moore, P.B., Araki T., and Ghose, S. (1982) Hyalotekite, a complex lead borosilicate: its crystal structure and the lone-pair effect on Pb(II). American Mineralogist, 67, 1012–1020.

Moore, P.B., Gupta, P.K.S., and Page, Y.L. (1989) Magnetoplumbite, $Pb^{2+}Fe^{3+}_{12}O_{19}$: Refinement and lone-pair splitting. American Mineralogist, 74, 1186–1194, 1989.

Nishida, N., Kimata, M., Kyono, A., Togawa, Y., Shimizu, M., and Hori, H. (1997) First finding of thallium-bearing ammonioleucite: A signal for the ultimate stage of the hydrothermal process and for a far-reaching effect from sea-water alteration of MORB. Annual Report of Institute of Geoscience, University of Tsukuba, 23, 35–41.

Noda, Y., Masumoto, K., Ohba, S., Saito, Y., Toriumi, K., Iwata, Y., and Shibuya, I. (1987) Temperature dependence of atomic thermal parameters of lead chalcogenides, PbS, PbSe and PbTe. Acta Crystallographica, C43, 1443–1445.

Noll, P.D., Newson, H.E., Leeman, W.P., and Ryan, J.G. (1996) The roll of hydrothermal fluids in the production of subduction zone magma: Evidence from siderophile and chalcophile trace elements and boron. Geochimica et Cosmochimica Acta, 60, 587–611.

Shannon, R.D. (1976) revised effective ionic radii and systematic studies of interatomic distances in halides and chalcogenides. Acta Crystallographica, A32, 751–767.

Sheldrick, G.M. (1997) SHELXL-97, program for crystal structure refinement. University of Göttingen, Germany.

Touboul, M., Bétourné, E., and Nowogrocki, G. (1997) Crystal structure of thallium triborate. Journal of Solid State Chemistry, 131, 370–373.

Wells, A.F. (1987) Structural inorganic chemistry, p. 1170–1173, Clarendon Press, Oxford.

West, A. R. (1999) Basic Solid State Chemistry, 2nd ed., p. 100–110. Wiley, New York .

Wintenberger, W. (1979) Etude de la structure cristallographique et magnetique de Cu_2FeGeS_4 et remarque sur la structure magnetique de Cu_2MnGeS_4. Materials Research Bulletin, 14, 1195–1202.

Zunic, T.B., Moélo, Y., Loncar, Z., and Micheelsen, H. (1994) Dorallcharite, $Tl_{0.8}K_{0.2}Fe_3(SO_4)_2(OH)_6$, a new member of the jarosite-alunite family. European Journal of Mineralogy, 6, 255–263.

MANUSCRIPT RECEIVED JUNE 10, 1999
MANUSCRIPT ACCEPTED APRIL 14, 2000
PAPER HANDLED BY JEFFREY E. POST